





Article

Study of the Synthetic Approach Influence in Ni/CeO₂-Based Catalysts for Methane Dry Reforming

Marco Pizzolato ¹, Giulia Da Pian ¹, Elena Ghedini ¹, Alessandro Di Michele ², Federica Menegazzo ¹, Giuseppe Cruciani ³ and Michela Signoretto ^{1,*}

¹ Department of Molecular Science and Nanosystems, Ca' Foscari University of Venice and INSTM RUVE, Via Torino 155, 30172 Venezia, Italy

² Department of Physics and Geology, Perugia University, Via Pascoli 1, 06123 Perugia, Italy

³ Department of Physics and Earth Science, Ferrara University, Via Saragat 1, 44122 Ferrara, Italy

* Correspondence: miky@unive.it

Abstract: This study focuses on the synthetic approach influence in morphostructural features and catalytic performances for Ni/CeO₂ catalysts. Incipient wetness impregnation, coprecipitation and nitrate combustion were studied as catalyst preparation approaches, and the materials were then tested at 700 °C for methane dry reforming (MDR). The morphostructural properties of the materials were deeply studied using several techniques, such as temperature programmed reduction (TPR), to investigate reducibility and support-metal interaction, N₂ physisorption to evaluate the porosity and the surface area, scanning electron microscopy (SEM) and X-ray diffraction (XRD) to estimate Ni dispersion, and temperature programmed oxidation (TPO) to identify the type and amount of coke formed on catalysts' surface after reaction. From the data obtained, coprecipitation turned out to be the most suitable technique for this application because this catalyst was able to reach 70% of CO₂ conversion and 30% methane conversion, with an H₂ yield of 15% and 30% yield of CO at the end of the 30 h test. Moreover, it was also the catalyst with the highest metal dispersion, the strongest interaction with the support, and the lowest coke deposition.

Keywords: Ni/CeO₂; co-precipitation; impregnation; nitrate combustion; methane dry reforming; hydrogen production; syngas



Citation: Pizzolato, M.; Da Pian, G.; Ghedini, E.; Di Michele, A.; Menegazzo, F.; Cruciani, G.; Signoretto, M. Study of the Synthetic Approach Influence in Ni/CeO₂-Based Catalysts for Methane Dry Reforming. *Reactions* **2022**, *3*, 634–647. <https://doi.org/10.3390/reactions3040043>

Academic Editor: Ioannis V. Yentekakis

Received: 25 October 2022

Accepted: 8 December 2022

Published: 16 December 2022

Publisher's Note: MDPI stays neutral with regard to jurisdictional claims in published maps and institutional affiliations.

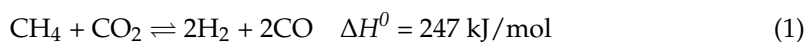


Copyright: © 2022 by the authors. Licensee MDPI, Basel, Switzerland. This article is an open access article distributed under the terms and conditions of the Creative Commons Attribution (CC BY) license (<https://creativecommons.org/licenses/by/4.0/>).

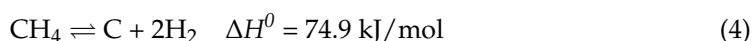
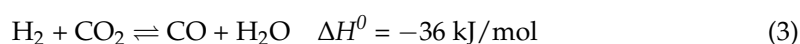
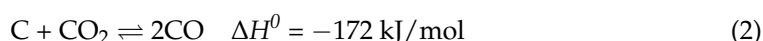
1. Introduction

In the last decades, the progressive greenhouse gas emissions in the atmosphere have triggered climate change [1]. The International Panel for Climate Change report, issued in February 2022, has strongly highlighted how climate change can negatively affect all the different ecosystems on our planet [2]. These scientific studies are pushing the need for a transition, and the research is now focused on the substitution of fossil-based energy sources with renewable ones. Biogas [3], which generally is obtained by anaerobic biomasses digestion, is one of the short-term viable options among different sustainable energy sources. The main components of biogas are CH₄, CO₂, and other gases such as H₂S, N₂, and H₂O [4]. Their utilization and conversion to higher-value products like syngas is also one of the key aspects: through reforming reactions it is possible to convert two greenhouse gases to highly requested industrial products. As a matter of fact, syngas is at the base of several processes, such as ammonia and methanol productions. At the industrial level, the most used ways to produce syngas nowadays are steam reforming (SR) or autothermal reforming (ATR) of natural gas [5,6]. However, these two processes can achieve only a 60% efficiency with a biogas-based feed [7]. Methane dry reforming (MDR) seems to be more appealing for this application compared to ATR and SR because it involves both CH₄ and CO₂ as reagents for the reaction. MDR is a highly endothermic reaction that

takes place above 600 °C and directly converts CO₂ and CH₄ to syngas [8] with a 1:1 ratio, according to Equation (1):



Despite the potentials of this reaction, it has not been yet applied on the industrial scale because of several reasons: First of all, this reaction is the most endothermic reforming reaction. Moreover, with the actual energetic scenario, it is not possible to afford a continuous CO₂ feed. Furthermore, this is a catalysed reaction, whose severe conditions lead to an high number of side reactions on the catalyst surface [9], such as reverse Boudouard reaction (Equation (2)), reverse water gas shift reaction (RWGS) (Equation (3)), and methane decomposition (Equation (4)):



Reactions (2) and (3) are responsible for variation in the H₂/CO ratio, whereas reaction (4) is involved in catalyst deactivation because it is responsible for coke formation. Therefore, it is evident how the design of a suitable catalyst is necessary to favour reagent activation and limit secondary reactions. A huge number of catalytic systems have been studied for this application, and they can be divided into two main groups: noble metal and non-noble metal supported catalysts. Moreira et al. [10] show the stability for over 180 h on stream with no evident deactivation of an Rh/Al₂O₃ catalyst. In fact, noble-metals-based catalysts such as platinum, rhodium, or ruthenium are well known for their higher activity and good resistance to coke deposition, but noble metal cost makes them non-feasible [11]. On the other hand, non-noble metals such as nickel and cobalt show good activity and low cost but poorer coke resistance than noble ones. A huge number of catalysts containing Ni were evaluated for MDR. Recently, Marinho et al. [12] studied a catalytic system based on Ni, Al₂O₃, and CeO₂ where the synergy between these three elements led to an increased resistance to coking of the active phase.

As has been stated, catalyst formulation is mandatory when non-noble metals are used for MDR, particularly to take advantage of the positive effects that support and promoters can give to catalyst activity. Among the different supports proposed in the literature, cerium oxide is one of the most studied. Ceria is well known for its peculiar basicity and redox properties, changing its oxidation state from Ce⁺⁴ to Ce⁺³, releasing oxygen ions reversibly [13]. These properties in MDR turned out to be essential to limit coke formation on the catalyst surface. Research is focused on doping CeO₂ with different metals, such as Zr [14], La [9], Sm [15], Gd [16], Fe [17], and Nd [18], to enhance its redox ability. These systems show good performances, but when it comes to an industrial scale-up, frequently, the costs of promoters and the scalability of the synthetic procedure are issues, and the catalyst is no longer economical [19].

The aim of this study is to compare for the first time, to the best of our knowledge, three easily scalable synthetic approaches: incipient wetness impregnation, coprecipitation, and nitrates combustion for the preparation of a non-doped Ni-CeO₂ catalyst with a 15 wt. % of Ni. The first two synthetic techniques are well known and established in industrial catalyst preparation, whereas nitrate combustion is an easy and cheap synthetic procedure for the preparation of advanced catalysts and nanomaterials. Using combustion-based routes, it is possible to produce nanopowders with homogeneous microstructure at shorter reaction times and lower temperatures. The main drawback of this synthetic approach is that the reaction and hence the final properties of the material are influenced by the nature of the organic complexing agent, stoichiometry of the solution, and metal ion complex stability. Moreover, the goal is to understand how the synthetic route influences the morphostructural properties of the catalyst and the catalytic behavior of the

materials and develop a stable, active, and selective catalyst for MDR. The morphostructural properties of these materials were deeply studied using several techniques, such as N_2 physisorption, to evaluate the porosity and the surface area, temperature programmed reduction (TPR) to investigate reducibility and support-metal interaction, X-ray diffraction (XRD) and scanning electron microscopy (SEM) to estimate Ni dispersion, and temperature programmed oxidation (TPO) to identify the type and amount of coke formed on catalysts' surface after reaction. The catalytic experiments were carried out in a fixed bed reactor at 700 °C. Temperature reaction was chosen based on reaction endothermicity; in this way it is possible to study catalysts' behavior under plausible and relevant industrial conditions.

2. Materials and Methods

All reagents were purchased from Sigma-Aldrich without further purifications.

2.1. Incipient Wetness Impregnation

Ceria support was synthesized by precipitation of an aqueous solution of $(NH_4)_2Ce(NO_3)_6$ using urea. A urea solution was prepared by dissolving 50 g of $CO(NH_2)_2$ in 100 mL of distilled water. A second solution of $(NH_4)_2Ce(NO_3)_6$ was prepared by dissolving 32 g of the salt in 100 mL of distilled water. The two solutions were mixed and maintained at 100 °C for 5 h. After that, the precipitate was washed with deionized water and dried at 110 °C for 18 h. Calcination was performed at 700 °C in air flow (30 mL/min) for 6 h. Nickel introduction on CeO_2 was done via incipient wetness impregnation with an aqueous solution of $Ni(NO_3)_2 \cdot 6H_2O$ in order to obtain 15 wt. % of nickel on the final material. After drying at 110 °C for 18 h, calcination was carried out at 700 °C in flowing air (30 mL/min) for 6 h.

2.2. Coprecipitation

The adequate amounts of $Ni(NO_3)_2 \cdot 6H_2O$ and $Ce(NO_3)_2 \cdot 6H_2O$ were dissolved in deionized water in order to obtain 15 wt. % of nickel on the final catalyst. This solution was added to an aqueous solution of NaOH 0.1 M with a rate of 1.3 mL/min. The pH of the final solution was kept constant at 10 with an agitation of 300 rpm, adding more NaOH when necessary during the process. After the precipitation, the suspension was aged for 12 h at room temperature, then filtered and washed with deionized water. After drying at 110 °C for 18 h, calcination was carried out at 700 °C in flowing air (30 mL/min) for 6 h.

2.3. Nitrates Combustion

The adequate amount of $Ni(NO_3)_2 \cdot 6H_2O$ and $Ce(NO_3)_2 \cdot 6H_2O$ were dissolved in deionized water in order to obtain 15 wt. % of nickel on the final catalyst. To this solution an excess of citric acid was added to substitute all nitrates in the metal's coordination sphere. The final solution was kept under agitation for 1 h at 300 rpm to obtain a homogeneous solution. Then, the solution was heated at 250 °C until a viscous gel was formed. After drying at 110 °C for 18 h, calcination was carried out at 700 °C in flowing air (30 mL/min) for 6 h.

Samples were denoted as NiCe (i), NiCe (c), and NiCe (n), respectively.

2.4. Characterization

Specific surface areas and pore-size distributions were determined by N_2 physisorption at -196 °C using a Tristar II Plus (Micromeritics). Samples were degassed prior to the analysis at 200 °C for 2 h using a vacuum degasser system. Surface area was calculated according to the B.E.T. equation [20], whereas pore size distribution was determined using the B.J.H. method [21], applied to the desorption branch of the N_2 isotherm.

Metallic tenor was determined with atomic absorption spectroscopy (AAS) using a Perkin Elmer AAnalyst 100. Prior to the analysis, each sample was mineralized in aqua regia under reflux for 5 h.

The temperature programme reduction (TPR) measurements were carried out in a quartz reactor, heating the catalyst in a reductive mixture flow (5% H₂/Ar; 40 mL/min) at a heating rate of 10 °C/min from 25 to 900 °C. H₂ consumption was recorded by a Gow-Mac TCD detector.

X-ray powder diffraction (XRD) analyses were performed using a Philips PW 1829/00 operated at 40 kV and 30 mA and equipped with a monochromator on the diffracted beam. The Rietveld refinement method was employed to do the quantitative phase analysis and crystal size determination of the support and metal phases.

Temperature programmed oxidation (TPO) was carried out in the same lab-made rig used for TPR. Samples were heated in an oxidative mixture flow (5% O₂/He) with a 10 °C/min rate from 25 to 900 °C.

SEM images of fresh and used samples were obtained using a scanning electron microscopy LEO 1525 ZEISS equipped with a field emission gun, after metallization with chromium (8nm). Images were acquired by Inlens detector, while a Bruker Quantax EDS detector was employed for elemental composition and chemical mapping.

2.5. Catalytic Tests

The catalytic tests were performed on a Microactivity Effi (Process Integral Development Eng & Tech) coupled to a gas chromatograph Agilent 8860 GC System. Prior to the catalytic test, each catalyst was pelletized into small pellets with an average size of 0.3–0.4 mm. The reactor was loaded with 1 mL of catalytic bed composed of 150 mg of catalyst mixed with SiC. Catalyst was reduced in situ under H₂ flow (30 mL/min) for 1 h at 500 °C. After reduction, the catalytic surface was cleaned by flowing He (180 mL/min) for 1 h. Activity tests were carried out at 700 °C for 30 h using a CH₄/CO₂/He reagent mixture (5/5/90) in a total flow of 200 mL/min. Regeneration was carried out at 600 °C with 10 mL/min of air for 1 h. After the analysis, conversions and yields were calculated using the following equations, where *f* stands for the flow rate of the gas:

$$\text{CH}_4 \text{ conversion \%} = [(f\text{CH}_4 \text{ in} - f\text{CH}_4 \text{ out})/f\text{CH}_4 \text{ in}] \cdot 100 \quad (5)$$

$$\text{CO}_2 \text{ conversion \%} = [(f\text{CO}_2 \text{ in} - f\text{CO}_2 \text{ out})/f\text{CO}_2 \text{ in}] \cdot 100 \quad (6)$$

$$\text{H}_2 \text{ yield \%} = (f\text{H}_2 \text{ out}/2 f\text{CH}_4 \text{ in}) \cdot 100 \quad (7)$$

$$\text{CO yield \%} = [f\text{CO out}/(f\text{CO}_2 \text{ in} + f\text{CH}_4 \text{ in})] \cdot 100 \quad (8)$$

$$\text{H}_2/\text{CO ratio} = f\text{H}_2 \text{ out}/f\text{CO out} \quad (9)$$

3. Results and Discussion

3.1. Characterizations

Preliminary characterizations were carried out to identify the morphostructural properties of the catalysts obtained by different synthetic approaches. Indeed, since in heterogeneous catalysts the reaction takes place on the catalyst's surface, high surface area, active phase's dispersion, and the interaction of active phase with support are important parameters that need to be determined, since this can hinder coke deposition and sinterization [22,23]. The results of N₂-physisorption concerning B.E.T. specific surface area and pore size distribution are reported in Table 1. Meanwhile, in Figure 1, N₂ adsorption-desorption isotherms and B.J.H. pore-size distributions are presented. According to IUPAC classification, all the isotherms are reconducible to type IV, although differences in surface area and pore network pattern are evident. Concerning the sample NiCe (i), the obtained isotherm is conducive to the one of pure CeO₂, in agreement with the used synthetic method [24]. It is possible to observe a very low value of surface area and pore volume that can be justified with Ni nanoparticles that have occluded the support's pores. NiCe (c) displays the highest surface area with a value of 34 m²/g. The isotherm presents a hysteresis loop positioned to high *p/p*⁰. It is possible that the synthetic approach has enhanced the interaction between the active phase and support, favoring the formation

of a pore network that is different from that of pure CeO_2 , with a higher value of surface area [25]. This is further confirmed by pore distribution centered at 10 nm. NiCe (n) shows an intermediated value of surface area if compared to the other two systems. The synthetic approach used for NiCe (n) has induced the formation of a more heterogeneous porosity pattern. As can be seen in Figure 1, the pore distribution for NiCe (n) catalyst is very wide and ranges from 5 to 50 nm. AAS analyses were also carried out to evaluate the effective amount of Ni inside the catalyst, and the results are reported in Table 1. Ni wt. % is in accordance with the nominal value chosen for these materials.

Table 1. Physical–chemical properties of Ni/CeO₂ catalysts and support (surface area calculated via B.E.T. equation; pore volume and average pore radius via B.J.H equation; real amount of nickel present in the catalysts determined via atomic adsorption).

	CeO ₂	NiCe (i)	NiCe (c)	NiCe (n)
Surface area (m ² /g)	49	8	34	18
Pore volume (cm ³ /g)	0.11	0.02	0.15	0.08
Average pore radius (nm)	4	4	10	7
Effective Ni amount (wt. %)	-	14.5	14.0	15.0

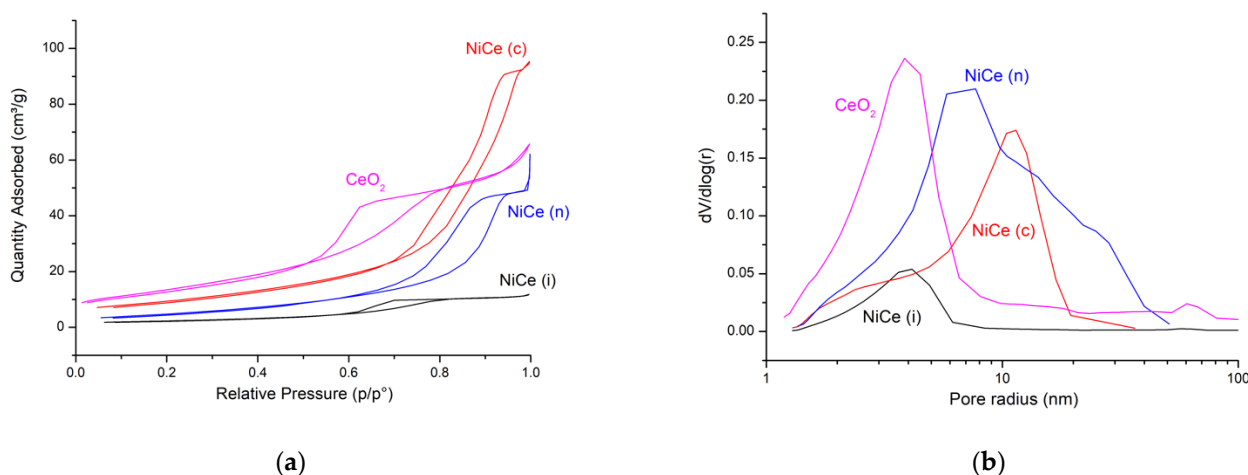


Figure 1. (a) N₂ physisorption isotherms of the three catalysts and support, (b) pore distribution of the three catalysts and support calculated using B.J.H. equation.

The TPR analyses reported in Figure 2 were carried out to understand the reducibility of the system and the interactions between active phase and support. Pure NiO presents only one reduction step going from Ni⁺² to Ni⁰; indeed, the presence of multiple peaks in all three samples can be ascribed to different strength interactions between the active phase and the support [26]. Metal-support interaction strength directly influences the reduction temperature of NiO, so for a higher Ni-Ce interaction, higher reduction temperatures are expected [27]. All three samples present two different species of NiO. The first refers to Ni that interacts less with the support in the form of superficial (Ni-O-Ce) species, as suggested by Lamonier et al. [28]. The second can be ascribed to NiO that has a strong interaction with CeO₂ [29]. In all catalysts, the fraction of low-interacting nickel is lower than the strong-interacting. NiCe (i) is the one with the lowest metal-support interaction; indeed, it is characterized by the lowest reduction temperatures among the three catalysts, with a temperature of 250 °C and 350 °C, respectively, for the first and second peak. This is in accord with the incipient wetness impregnation technique, which, generally, does not favor a strong metal-support interaction [30]. NiCe I and NiCe (n) are characterized by a 50 °C higher reduction temperature for both of the peaks if compared to NiCe (i). This confirms, furthermore, the best interaction that can be achieved using these synthetic approaches rather than incipient wetness impregnation. The shoulder at 480 °C can be

ascribed to superficial reduction of CeO_2 reduction to Ce_2O_3 , whereas the peak around 800°C is due to bulk CeO_2 reduction [31].

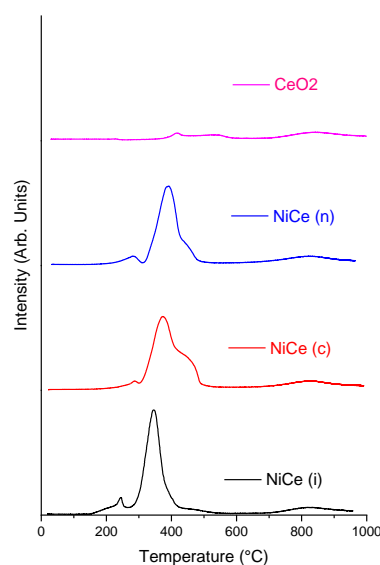


Figure 2. TPR profiles of the catalysts and pure CeO_2 as reference.

SEM analyses were made to investigate the influence of the synthetic approach on the catalysts' morphology. The results report that the three samples are very different from each other. (Figure 3). NiCe (i) is the most heterogeneous material, presenting a different shape and particle size. NiCe (c) is the finest material, with a smaller homogeneous aggregates size around $10\ \mu\text{m}$. NiCe (n) is the most peculiar sample, with ceramic features caused by gas evolution during the combustion reaction used for the synthesis [32].

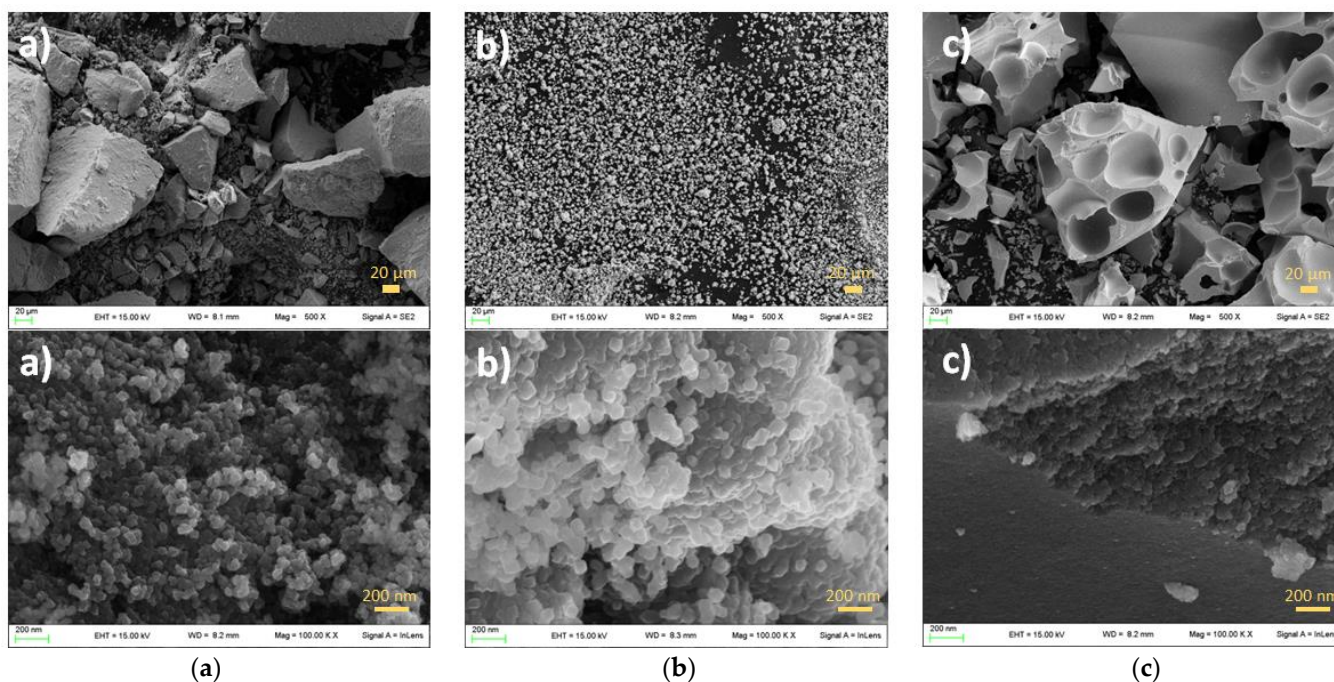


Figure 3. SEM images of the catalysts (a) NiCe (i); (b) NiCe (c); (c) NiCe (n).

The XRD spectra of the catalysts (Figure 4) were carried out to evaluate NiO nanoparticles' dimension and crystalline phases present in the materials. From the diffraction patterns, only pure fluorite-type CeO_2 and bunsenite-type NiO were identified for

the three samples. As reported in Table 2, the CeO₂:NiO weight ratio in all three catalysts is constant, with a value of 80:20. Considering the contribution of oxygen in the weight percentage of the oxide, these data are in accordance with AAS analyses performed for Ni determination. Concerning the crystallite dimension, some differences among the catalysts are evident. NiCe (c) has the most dispersed NiO with an average dimension of 7 nm, followed by NiCe (n) with 13 nm. The biggest NiO crystallites are found in NiCe (i), with a dimension of 30 nm.

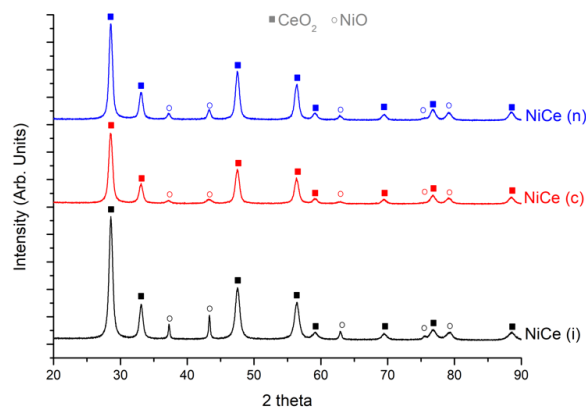


Figure 4. XRD spectra of the catalysts.

Table 2. NiO crystallite dimensions obtained by XRD analysis using the Scherrer equation; phase composition of the catalysts determined via XRD.

Catalyst	NiO Dimensions (nm)	NiO wt. %	CeO ₂ wt. %
NiCe (i)	30	20	80
NiCe (c)	7	21	79
NiCe (n)	13	21	79

3.2. Catalytic Tests

As previously stated, MDR is a promising endothermic process for syngas production from biogas [33]. For these reasons, the reactions tests were carried out at 700 °C for 30 h with a GHSV of 12,000 h⁻¹. Moreover, for each system, conversions of CH₄, CO₂ and H₂/CO have been calculated. A variation in this ratio can be ascribed to progressive catalyst deactivation [34].

Observing the trend of conversions of methane and carbon dioxide for each sample tested (Figure 5), it is clear how the deactivation occurs more slowly in catalysts made by the combustion method and coprecipitation.

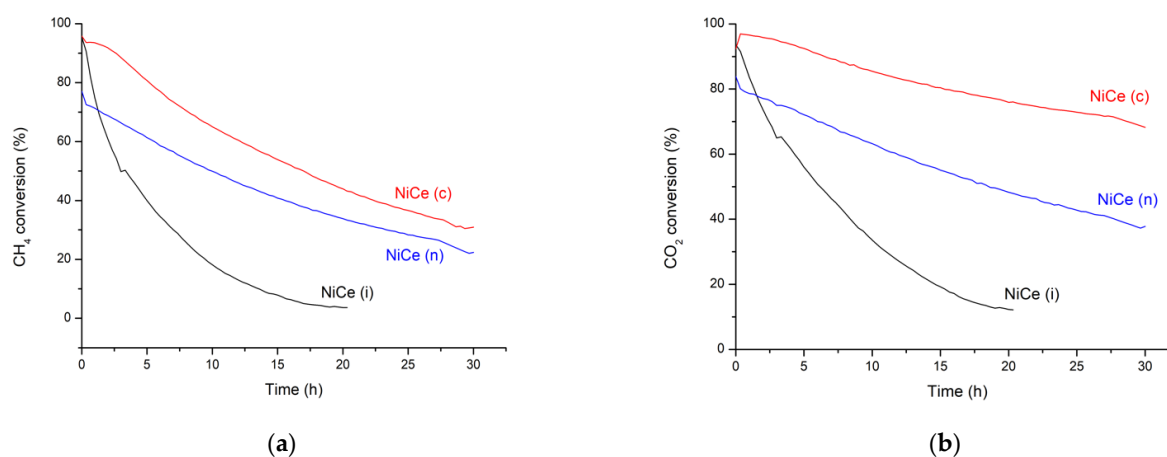


Figure 5. CH₄ conversion (a) and CO₂ conversion (b) of the three catalysts at reaction conditions.

In fact, NiCe (i) has a rapid drop-in activity, passing from an initial 90% to 15% in only a few hours. For NiCe (c) and NiCe (n), indeed, conversion values are optimal in the first hours and the loss after 30 h on stream is far less low, with an average 30% conversion of methane and 70% conversion of carbon dioxide. This agrees with characterization data previously described: the better Ni dispersion and higher surface area of NiCe catalyst give an improved activity and less carbon deposition. To confirm this best performance of NiCe (c), it is possible to compare the trends in H₂ and CO yield for the three catalysts, too (Figure S1). NiCe (i) is the less active among the three samples, reaching only 10% yield of both H₂ and CO after only 15 h. On the other hand, NiCe (c) and NiCe (n) are characterized by a rather constant trend in activity loss. In particular, the initial activity of NiCe (i) is 50% H₂ yield and 65% CO yield, but these optimal values drastically decrease very rapidly after the first hours. The progressive deactivation of the catalyst is highlighted also by the H₂/CO ratio (Figure 6), where after an initial decrease, the value progressively increases up to 1.0. This indicates that there is less CO production, so it could mean that coke deposition is favoured, leading to a faster catalyst deactivation. As a matter of fact, in this system, the CH₄ decomposition reaction (Equation (4)) is very competitive with the MDR reaction and leads to coke formation on the catalyst's surface [35]. NiCe (c) is the most active catalyst, achieving a CO and H₂ yield, respectively, of 65% and 45% in the first hours; moreover, it presents the lowest deactivation degree during the catalytic tests, presenting still a 20% yield of H₂ and a 30% yield of CO after 30 h on stream. NiCe (n) possessed a similar activity trend compared to NiCe (c), but with an overall lower activity, starting from 40% H₂ yield and 55% CO yield, and reaching, after 30 h, respectively, 20% and 27%. The stronger metal-support interaction and higher nickel dispersion of NiCe (c) and NiCe (n) compared to NiCe (i) caused a higher resistance to coke deposition and therefore to catalyst deactivation. Therefore, the best catalyst is confirmed to be NiCe (c). Moreover, even if it is always difficult compare different catalytic rigs, this catalyst performs better than others previously reported in the literature, both on non-doped Ni/CeO₂, obtained by different synthetic approaches, and on doped Ni/CeO₂. For example, Yahi et al. [36] reported a Ni/CeO₂ catalyst prepared via microemulsion that showed no activity toward MDR because of larger particles size (34 nm) and/or NiO cubic structure instead of monoclinic. As well, Kambolis et al. [37] reported a Ni/CeO₂-ZrO₂ catalyst, where Ni was introduced via incipient wetness impregnation, that showed lower activity compared to those studied in this work, despite the introduction of Zr as support structural promoter to enhance the oxygen deficiency on the support.

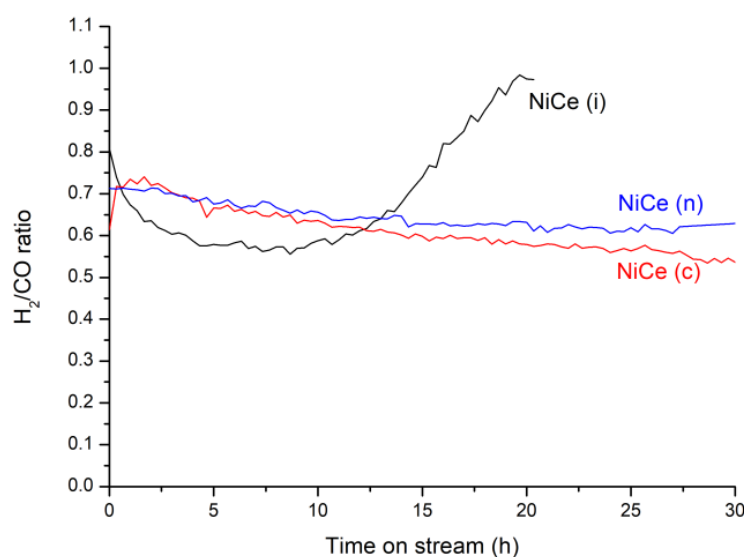


Figure 6. H₂/CO ratio of three catalysts in reaction conditions.

In Table 3, there are reported some studies on Ni-ceria-based catalysts, synthesized by different methodologies and amount of nickel and investigated in the same temperature range. This is useful to make a comparison and evaluate whether the diversity in the activity trends obtained in this work can be traced back to the synthetic methodology. A complete comparison between different Ni/CeO₂ catalysts present in the literature and materials here presented cannot be done due to the lack of standard conditions in MDR tests. Indeed, the conditions of reaction and amount of active metal phase are often different, but the most similar and recent to the ones used in this work were selected.

Table 3. Activity in terms of CH₄ and CO₂ conversion of Ni/CeO₂ catalysts, prepared with different methods and similar amount of Ni. The data refer to the start of reaction.

Catalyst	Ni wt. %	Synthetic Method	Conversion (%)		H ₂ /CO Ratio	Temp. (°C)	Ref.
			CH ₄	CO ₂			
NiCe (c)	14	Coprecipitation	95	97	0.6	700	This work
Ni/CeO ₂ flakes	10	Impregnation	15	42	0.5	700	[38]
Ni/CeO ₂ Nanoparticles	10	Impregnation	18	45	0.6	700	[38]
Ni/CeO ₂	8	Wet impregnation	80	75	Lower than 1.0	700	[39]
Ni/CeO ₂	13	Combustion synthesis	90	-	0.95	750	[40]
Ni/CeO ₂	9.5	Wet Impregnation	65	65	2	700	[41]
Ni/commercial CeO ₂	7.5	Wet impregnation	45	45	2	700	[41]
CeNi _{0.3} O _y	7.5	Coprecipitation	5	25	2	700	[41]
Ni/CeO ₂	10	Wetness Impregnation	35	65	0.65	700	[42]
Ni/@CeO ₂	10	Self-assembly	55	65	0.8	800	[43]
Ni/CeO ₂	10	Incipient wetness impregnation	60	70	0.8	800	[43]
Ni/CeO ₂	7.5	Surfactant assisted coprecipitation	70	75	0.8	700	[43]

The interesting fact is that, even if tested at the same temperature conditions, the conversion results of CH₄ and CO₂ at the beginning of the reactions are very different from each other. Although the amount of nickel is not exactly the same, it is clear that the synthetic methodology, and therefore the structural characteristics of the material, are fundamental in assessing the activity of a catalyst. This can also be highlighted by the fact that in the two cases where higher temperatures are used (800 °C), the conversions are not better than those obtained at 700 °C with other samples, which would be expected given the endothermicity of the MDR reaction. The only case in which there are conversions comparable to that of the present work is for the sample tested at 750 °C (90% for CH₄), which also contains a similar amount of Ni (13% against 14%). The literature therefore confirms the different activity trends observed among the catalysts, highlighting the fact that the selection of the proper synthetic approach is crucial to maximize the catalytic activity. In addition, in this case, higher conversions were achieved without the addition of promoters in the samples, frequently added in most of the recent studies reported in the literature [12,44–46].

3.3. Characterization of Spent Catalyst

The spent samples were deeply investigated using SEM, EDX, and TPO analyses to understand the reasons of catalytic behaviour. The spent catalysts' SEM images are reported in Figure 7. As can be seen, the surface of NiCe (i) is completely covered by coke compared to the fresh sample reported in Figure 3. This agrees with catalytic test, in which a rapid deactivation was observed. However, NiCe (c) and NiCe (n) were gradually deactivated. As can be seen, NiCe (c) and NiCe (n) after 30 h of reaction have a partially free surface,

whereas that of NiCe (i) is completely covered by carbon nanotubes. EDX analyses of spent catalysts (Figure 8) further confirm the presence of carbon on the catalysts' surface, but with a different weight % ratio between C and Ni. In particular, in spent NiCe (i) catalyst, the amount of carbon is higher than spent NiCe (c) and spent NiCe (n), suggesting that the stronger interaction of Ni with support in NiCe (c) and NiCe (n) has hindered carbon deposition favouring their stability.

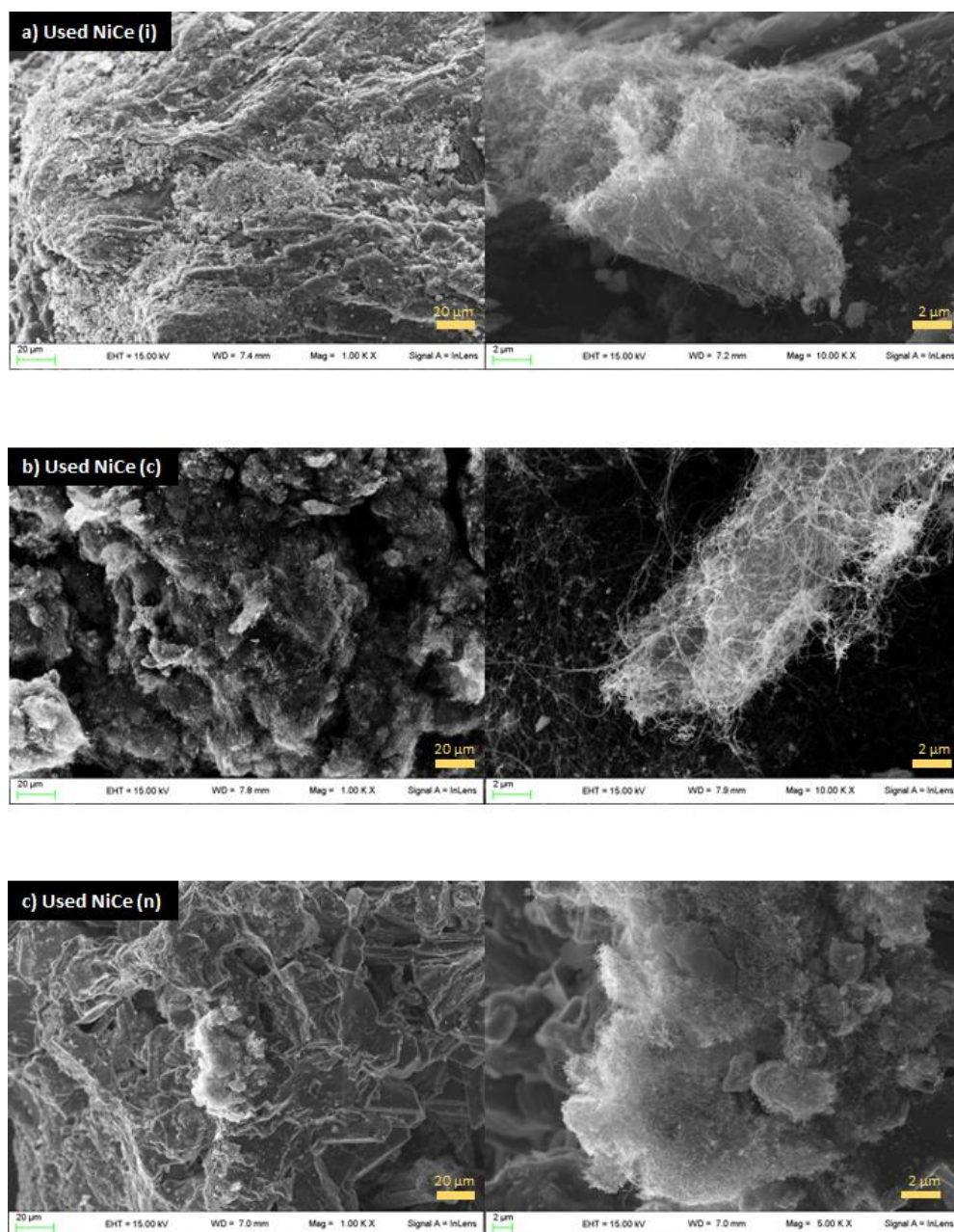


Figure 7. SEM analysis on spent catalysts: (a) used NiCe (i); (b) used NiCe (c); (c) used NiCe (n).

TPO analyses (Figure 9) were carried out to further evaluate the type of coke deposition on the catalysts' surface. As can be seen, NiCe (i) has a main peak centered at 800 °C with a shoulder at 900 °C. These peaks can be ascribed to two different carbonaceous species—respectively, to graphite and graphene [47]. NiCe (n), on the contrary, presents only one type of carbonaceous species at 800 °C, which can be attributed to graphitic carbon. NiCe (c) is the catalyst with the lowest coke removal temperature; this makes this system even more appealing for a hypothetical industrial application because it could

be possible to regenerate it at 400–600 °C. As a matter of fact, carbonaceous species on this catalyst refers to amorphous carbon mixed with multi-walled carbon nanotubes [48]. Further analyses will be performed in order to optimize the regeneration treatment.

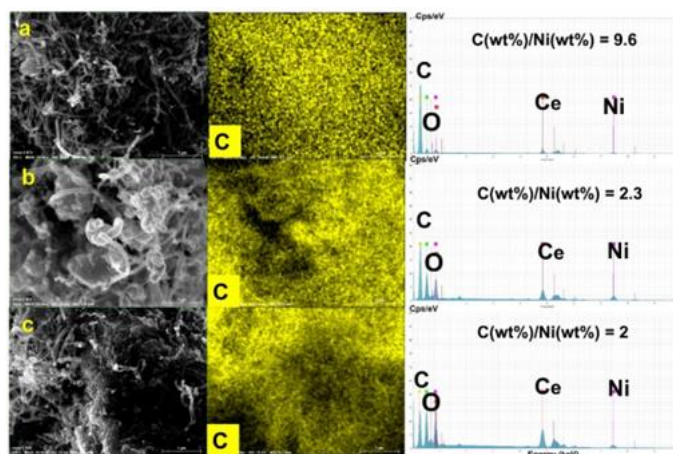


Figure 8. Carbon Mapping and EDX spectra of spent catalysts: (a) used NiCe (i); (b) used NiCe (c); (c) used NiCe (n).

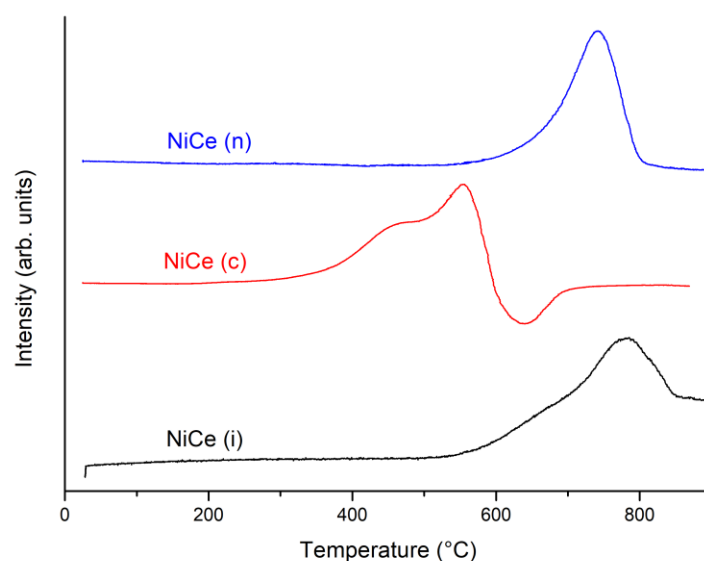


Figure 9. TPO analyses of the spent samples.

4. Conclusions

A synthetic approach has a strong effect on the activity and stability of catalysts. Higher surface area coupled with high nanoparticles dispersion and strong metal-support interaction are mandatory for a robust MDR catalyst. These features are directly connected with the preparation route chosen. In particular, incipient wetness impregnation led to a catalyst where Ni dispersion is low and with weak metal-support interaction, as shown by XRD and TPR analyses. This caused a rapid deactivation of the catalyst due to graphitic coke formation on the Ni surface, as highlighted by SEM and TPO analyses. Compared to this extensively used technique for catalysts' preparation, coprecipitation and nitrate combustion approaches turned out to be more suitable for a MDR Ni/CeO₂-based catalyst, still being easy and scalable synthetic routes. Samples prepared by coprecipitation possess the highest surface area, highest metal-support interaction, highest Ni dispersion, best activity, lowest coke formation rate, and lowest regeneration temperature for a possible future regeneration. The synthetic approach led to the formation of the best synergic

interaction between active phase and support. This is due to the higher interaction that Ni and Ce have during the precipitation, giving them the ability to form a hybrid network where the redox ability of cerium dioxide and its strong interaction with nickel nanoparticles enhanced the activity, avoiding coke deposition.

Supplementary Materials: The following supporting information can be downloaded at: <https://www.mdpi.com/article/10.3390/reactions3040043/s1>, Figure S1: 1 H₂ yield (a) and CO yield (b) of the three catalysts at reaction conditions (700 °C; GHSV 12,000 h⁻¹)

Author Contributions: Conceptualization, M.P. and G.D.P.; methodology M.P., G.D.P., A.D.M. and G.C.; data curation, M.P., G.D.P., E.G., F.M. and M.S.; writing—review and editing, M.S. and F.M.; supervision, M.S.; All authors have read and agreed to the published version of the manuscript.

Funding: This research received no external funding.

Acknowledgments: Tania Fantinel is acknowledged for her excellent technical assistance. Francesca Langiano is gratefully acknowledged for her practical collaboration within this work. M.P. and G.D.P. thank the Doctorate in Chemistry of UniTS.

Conflicts of Interest: The authors declare no conflict of interest.

References

1. Thompson, L.G. Climate Change: The Evidence and Our Options. *Behav. Anal.* **2010**, *33*, 153–170. [CrossRef] [PubMed]
2. AR6 Climate Change 2022: Impacts, Adaptation and Vulnerability—IPCC. Available online: <https://www.ipcc.ch/report/sixth-assessment-report-working-group-ii/> (accessed on 26 April 2022).
3. Naik, S.N.; Goud, V.V.; Rout, P.K.; Dalai, A.K. Production of First and Second Generation Biofuels: A Comprehensive Review. *Renew. Sust. Energ. Rev.* **2010**, *14*, 578–597. [CrossRef]
4. Yang, L.; Ge, X.; Wan, C.; Yu, F.; Li, Y. Progress and Perspectives in Converting Biogas to Transportation Fuels. *Renew. Sust. Energ. Rev.* **2014**, *40*, 1133–1152. [CrossRef]
5. Boyano, A.; Morosuk, T.; Blanco-Marigorta, A.M.; Tsatsaronis, G. Conventional and Advanced Exergoenvironmental Analysis of a Steam Methane Reforming Reactor for Hydrogen Production. *J. Clean. Prod.* **2012**, *20*, 152–160. [CrossRef]
6. Rostrup-Nielsen, J.R.; Sehested, J.; Nørskov, J.K. Hydrogen and Synthesis Gas by Steam- and CO₂ Reforming. *Adv. Catal.* **2002**, *47*, 65–139. [CrossRef]
7. Minutillo, M.; Perna, A.; Sorce, A. Green Hydrogen Production Plants via Biogas Steam and Autothermal Reforming Processes: Energy and Exergy Analyses. *Appl. Energy* **2020**, *277*, 115452. [CrossRef]
8. Wittich, K.; Krämer, M.; Bottke, N.; Schunk, S.A. Catalytic Dry Reforming of Methane: Insights from Model Systems. *ChemCatChem.* **2020**, *12*, 2130–2147. [CrossRef]
9. Pizzolitto, C.; Pupulin, E.; Menegazzo, F.; Ghedini, E.; di Michele, A.; Mattarelli, M.; Cruciani, G.; Signoretto, M. Nickel Based Catalysts for Methane Dry Reforming: Effect of Supports on Catalytic Activity and Stability. *Int. J. Hydrogen Energy* **2019**, *44*, 28065–28076. [CrossRef]
10. de Araújo Moreira, T.G.; de Carvalho Filho, J.F.S.; Carvalho, Y.; de Almeida, J.M.A.R.; Nothaft Romano, P.; Falabella Sousa-Aguiar, E. Highly Stable Low Noble Metal Content Rhodium-Based Catalyst for the Dry Reforming of Methane. *Fuel* **2021**, *287*, 119536. [CrossRef]
11. Menegazzo, F.; Signoretto, M.; Pinna, F.; Canton, P.; Pernicone, N. Optimization of Bimetallic Dry Reforming Catalysts by Temperature Programmed Reaction. *Appl. Catal. A Gen.* **2012**, *439–440*, 80–87. [CrossRef]
12. Marinho, A.L.A.; Toniolo, F.S.; Noronha, F.B.; Epron, F.; Duprez, D.; Bion, N. Highly Active and Stable Ni Dispersed on Mesoporous CeO₂-Al₂O₃ Catalysts for Production of Syngas by Dry Reforming of Methane. *Appl. Catal. B Environ.* **2021**, *281*, 119459. [CrossRef]
13. Melchionna, M.; Trovarelli, A.; Fornasiero, P. Synthesis and Properties of Cerium Oxide-Based Materials. In *Cerium Oxide (CeO₂): Synthesis, Properties and Applications*, 1st ed.; Scire, S., Palmisano, L., Eds.; Elsevier: Amsterdam, The Netherlands, 2020; pp. 13–43. [CrossRef]
14. Zhang, F.; Liu, Z.; Chen, X.; Rui, N.; Betancourt, L.E.; Lin, L.; Xu, W.; Sun, C.J.; Abeykoon, A.M.M.; Rodriguez, J.A.; et al. Effects of Zr Doping into Ceria for the Dry Reforming of Methane over Ni/CeZrO₂ Catalysts: In Situ Studies with XRD, XAFS, and AP-XPS. *ACS Catal.* **2020**, *10*, 3274–3284. [CrossRef]
15. Chien, A.C.; Ye, N.J.; Huang, C.W.; Tseng, I.H. Studies of Nickel/Samarium-Doped Ceria for Catalytic Partial Oxidation of Methane and Effect of Oxygen Vacancy. *Catalysts* **2021**, *11*, 731–743. [CrossRef]
16. Gurav, H.R.; Dama, S.; Samuel, V.; Chilukuri, S. Influence of Preparation Method on Activity and Stability of Ni Catalysts Supported on Gd Doped Ceria in Dry Reforming of Methane. *J. CO₂ Util.* **2017**, *20*, 357–367. [CrossRef]
17. Odedairo, T.; Ma, J.; Chen, J.; Wang, S.; Zhu, Z. Influences of Doping Cr/Fe/Ta on the Performance of Ni/CeO₂ Catalyst under Microwave Irradiation in Dry Reforming of CH₄. *J. Solid State Chem.* **2016**, *233*, 166–177. [CrossRef]

18. Lara-García, H.A.; Araiza, D.G.; Méndez-Galván, M.; Tehuacanero-Cuapa, S.; Gómez-Cortés, A.; Díaz, G. Dry Reforming of Methane over Nickel Supported on Nd–Ceria: Enhancement of the Catalytic Properties and Coke Resistance. *RSC Adv.* **2020**, *10*, 33059–33070. [[CrossRef](#)]
19. Mitchell, S.; Michels, N.L.; Pérez-Ramírez, J. From Powder to Technical Body: The Undervalued Science of Catalyst Scale Up. *Chem. Soc. Rev.* **2013**, *42*, 6094–6112. [[CrossRef](#)]
20. Brunauer, S.; Emmett, P.H.; Teller, E. Adsorption of Gases in Multimolecular Layers. *J. Am. Chem. Soc.* **2002**, *60*, 309–319. [[CrossRef](#)]
21. Barrett, E.P.; Joyner, L.G.; Halenda, P.P. The Determination of Pore Volume and Area Distributions in Porous Substances. I. Computations from Nitrogen Isotherms. *J. Am. Chem. Soc.* **2002**, *73*, 373–380. [[CrossRef](#)]
22. Manzoli, M.; Menegazzo, F.; Signoretto, M.; Cruciani, G.; Pinna, F. Effects of Synthetic Parameters on the Catalytic Performance of Au/CeO₂ for Furfural Oxidative Esterification. *J. Catal.* **2015**, *330*, 465–473. [[CrossRef](#)]
23. Menegazzo, F.; Burti, P.; Signoretto, M.; Manzoli, M.; Vankova, S.; Boccuzzi, F.; Pinna, F.; Strukul, G. Effect of the Addition of Au in Zirconia and Ceria Supported Pd Catalysts for the Direct Synthesis of Hydrogen Peroxide. *J. Catal.* **2008**, *257*, 369–381. [[CrossRef](#)]
24. Menegazzo, F.; Pizzolitto, C.; Ghedini, E.; di Michele, A.; Cruciani, G.; Signoretto, M. Development of La Doped Ni/CeO₂ for CH₄/CO₂ Reforming. *J. Carbon Res.* **2018**, *4*, 60–76. [[CrossRef](#)]
25. Sepehri, S.; Rezaei, M.; Wang, Y.; Younesi, A.; Arandiyani, H. The Evaluation of Autothermal Methane Reforming for Hydrogen Production over Ni/CeO₂ Catalysts. *Int. J. Hydrogen Energy* **2018**, *43*, 22340–22346. [[CrossRef](#)]
26. Khatri, J.; Fakeeha, A.H.; Kasim, S.O.; Lanre, M.S.; Abasaeed, A.E.; Ibrahim, A.A.; Kumar, R.; Al-Fatesh, A.S. Ceria Promoted Phosphate-Zirconia Supported Ni Catalyst for Hydrogen Rich Syngas Production through Dry Reforming of Methane. *Int. J. Energy Res.* **2021**, *45*, 19289–19302. [[CrossRef](#)]
27. Pizzolitto, C.; Menegazzo, F.; Ghedini, E.; Innocenti, G.; di Michele, A.; Cruciani, G.; Cavani, F.; Signoretto, M. Increase of Ceria Redox Ability by Lanthanum Addition on Ni Based Catalysts for Hydrogen Production. *ACS Sustain. Chem. Eng.* **2018**, *6*, 13867–13876. [[CrossRef](#)]
28. Lamonier, C.; Ponchel, A.; D’Huysser, A.; Jalowiecki-Duhamel, L. Studies of the Cerium-Metal–Oxygen–Hydrogen System (Metal=Cu, Ni). *Catal. Today* **1999**, *50*, 247–259. [[CrossRef](#)]
29. Li, L.; Jiang, B.; Tang, D.; Zheng, Z.; Zhao, C. Hydrogen Production from Chemical Looping Reforming of Ethanol Using Ni/CeO₂ Nanorod Oxygen Carrier. *Catalysts* **2018**, *8*, 257. [[CrossRef](#)]
30. Matus, E.V.; Shlyakhtina, A.S.; Sukhova, O.B.; Ismagilov, I.Z.; Ushakov, V.A.; Yashnik, S.A.; Nikitin, A.P.; Bharali, P.; Kerzhentsev, M.A.; Ismagilov, Z.R. Effect of Preparation Methods on the Physicochemical and Functional Properties of Ni/CeO₂ Catalysts. *Kinet. Catal.* **2019**, *60*, 221–230. [[CrossRef](#)]
31. Vita, A.; Italiano, C.; Fabiano, C.; Laganà, M.; Pino, L. Influence of Ce-Precursor and Fuel on Structure and Catalytic Activity of Combustion Synthesized Ni/CeO₂ Catalysts for Biogas Oxidative Steam Reforming. *Mater. Chem. Phys.* **2015**, *163*, 337–347. [[CrossRef](#)]
32. Palneedi, H.; Mangam, V.; Das, S.; Das, K. Effect of Fuel-to-Nitrate Ratio on the Powder Characteristics of Nanosized CeO₂ Synthesized by Mixed Fuel Combustion Method. *J. Alloys Compd.* **2011**, *509*, 9912–9918. [[CrossRef](#)]
33. Zhao, K.; Hou, X.; Norton, M.G.; Ha, S. Application of a NiMo–Ce_{0.5}Zr_{0.5}O_{2-Δ} Catalyst for Solid Oxide Fuel Cells Running on Gasoline. *J. Power Source* **2019**, *435*, 226732. [[CrossRef](#)]
34. Odedairo, T.; Chen, J.; Zhu, Z. Metal-Support Interface of a Novel Ni–CeO₂ Catalyst for Dry Reforming of Methane. *Catal. Commun.* **2013**, *31*, 25–31. [[CrossRef](#)]
35. Chein, R.; Yang, Z. Experimental Study on Dry Reforming of Biogas for Syngas Production over Ni-Based Catalysts. *ACS Omega* **2019**, *4*, 20911–20922. [[CrossRef](#)] [[PubMed](#)]
36. Yahi, N.; Menad, S.; Rodríguez-Ramos, I. Dry Reforming of Methane over Ni/CeO₂ Catalysts Prepared by Three Different Methods. *Green Process. Synth.* **2015**, *4*, 479–486. [[CrossRef](#)]
37. Kambolis, A.; Matralis, H.; Trovarelli, A.; Papadopoulou, C. Ni/CeO₂-ZrO₂ Catalysts for the Dry Reforming of Methane. *Appl. Catal. A Gen.* **2010**, *377*, 16–26. [[CrossRef](#)]
38. Rood, S.C.; Ahmet, H.B.; Gomez-Ramon, A.; Torrente-Murciano, L.; Reina, T.R.; Eslava, S. Enhanced Ceria Nanoflakes Using Graphene Oxide as a Sacrificial Template for CO Oxidation and Dry Reforming of Methane. *Appl. Catal. B Environ.* **2019**, *242*, 358–368. [[CrossRef](#)]
39. Ay, H.; Üner, D. Dry Reforming of Methane over CeO₂ Supported Ni, Co and Ni-Co Catalysts. *Appl. Catal. B Environ.* **2015**, *179*, 128–138. [[CrossRef](#)]
40. Gonzalez-Delacruz, V.M.; Ternero, F.; Pereñíguez, R.; Caballero, A.; Holgado, J.P. Study of Nanostructured Ni/CeO₂ Catalysts Prepared by Combustion Synthesis in Dry Reforming of Methane. *Appl. Catal. A Gen.* **2010**, *384*, 1–9. [[CrossRef](#)]
41. Guerrero-Caballero, J.; Kane, T.; Haidar, N.; Jalowiecki-Duhamel, L.; Löfberg, A. Ni, Co, Fe Supported on Ceria and Zr Doped Ceria as Oxygen Carriers for Chemical Looping Dry Reforming of Methane. *Catal.* **2019**, *333*, 251–258. [[CrossRef](#)]
42. Grabchenko, M.; Pantaleo, G.; Puleo, F.; Kharlamova, T.S.; Zaikovskii, V.I.; Vodyankina, O.; Liotta, L.F. Design of Ni-Based Catalysts Supported over Binary La–Ce Oxides: Influence of La/Ce Ratio on the Catalytic Performances in DRM. *Catal. Today* **2021**, *382*, 71–81. [[CrossRef](#)]

43. Marinho, A.L.A.; Rabelo-Neto, R.C.; Epron, F.; Bion, N.; Toniolo, F.S.; Noronha, F.B. Embedded Ni Nanoparticles in CeZrO₂ as Stable Catalyst for Dry Reforming of Methane. *Appl. Catal. B Environ.* **2020**, *268*, 118387. [[CrossRef](#)]
44. Luisetto, I.; Tuti, S.; di Bartolomeo, E. Co and Ni Supported on CeO₂ as Selective Bimetallic Catalyst for Dry Reforming of Methane. *Int. J. Hydrogen Energy* **2012**, *37*, 15992–15999. [[CrossRef](#)]
45. Cesario, M.R.; Souza, G.S.; Loureiro, F.J.A.; Araújo, A.J.M.; Grilo, J.P.F.; Aouad, S.; Tidahy, H.L.; Macedo, D.A.; Fagg, D.P.; Gennequin, C.; et al. Synthesis of Co–Ni and Cu–Ni Based-Catalysts for Dry Reforming of Methane as Potential Components for SOFC Anodes. *Ceram. Int.* **2021**, *47*, 33191–33201. [[CrossRef](#)]
46. Majewski, A.J.; Singh, S.K.; Labhasetwar, N.K.; Steinberger-Wilckens, R. Nickel–Molybdenum Catalysts for Combined Solid Oxide Fuel Cell Internal Steam and Dry Reforming. *Chem. Eng. Sci.* **2021**, *232*, 116341. [[CrossRef](#)]
47. da Fonseca, R.O.; Pongeggi, A.R.; Rabelo-Neto, R.C.; Simões, R.C.C.; Mattos, L.V.; Noronha, F.B. Controlling Carbon Formation over Ni/CeO₂ Catalyst for Dry Reforming of CH₄ by Tuning Ni Crystallite Size and Oxygen Vacancies of the Support. *J. CO₂ Util.* **2022**, *57*, 101880. [[CrossRef](#)]
48. Jang, W.J.; Shim, J.O.; Kim, H.M.; Yoo, S.Y.; Roh, H.S. A Review on Dry Reforming of Methane in Aspect of Catalytic Properties. *Catal. Today* **2019**, *324*, 15–26. [[CrossRef](#)]